Pinching relativistic electrons in the quantum degenerate plasmas to enhance the fast heating

Y.-H. Li,[1,2,3] D. Wu,[3,*] and J. Zhang[1,2,3,†]

[1] *Institute of Physics, Chinese Academy of Sciences, Beijing 100190, People's Republic of China*
[2] *University of Chinese Academy of Sciences, Beijing 100049, People's Republic of China*
[3] *Key Laboratory for Laser Plasmas and Department of Physics and Astronomy, and Collaborative Innovation Center of IFSA (CICIFSA), Shanghai Jiao Tong University, Shanghai 200240, People's Republic of China*

(Dated: February 24, 2025)

The transport process of a relativistic electron beam (REB) in high density and degenerate plasmas holds significant importance for fast ignition. In this study, we have formulated a comprehensive theoretical model to address this issue, incorporating quantum degeneracy, charged particle collisions, and effects of electromagnetic (EB) fields. We model the fuel as a uniform density region and specially focus on the effect of quantum degeneracy during the transport of the REB, which leads to the rapid growth of self-generated EB field and a subsequently significant self-organized pinching of the REB. Through our newly developed hybrid particle-in-cell simulations, we have observed a two-fold enhancement of the heating efficiency of REB than previous intuitive expectation. This finding provides a promising theoretical framework for exploring the degeneracy effect and the enhanced self-generated EB field in the dense plasma for fast ignition, and is also linked to a wide array of ultra-intense laser-based applications.

I. INTRODUCTION

Recently, ignition and burning of Deuterium–Tritium (DT) plasmas [1, 2] in the laboratory have been successively achieved in inertial confinement fusion (ICF) [3] experiments conducted at the National Ignition Facility (NIF). This achievement has inspired worldwide research efforts in ICF, especially on higher heating efficiency and more stable operation of ICF process to realize the dream of fusion energy for a carbon free future world. Notably, the fast ignition (FI) approach [4], characterized by high heating efficiency with relaxed requirement for symmetrical implosion, have garnered significant attention.

In the FI approach, a relativistic electron beam (REB) is generated by the picosecond laser pulse, and injected into the isochoric pre-compressed fuel core to raise its temperature rapidly. During the fast heating phase, the transport efficiency of REB in high density and degenerate plasmas is an inevitable challenge [5, 6]. To enhance the efficiency of energy transport from the REB to the pre-compressed fuel, the REB must be injected sufficiently close to the high density core of the fuel. However, the outward expansion of the ablation-induced corona displaces the critical density, where the REB is generated, further from the high density core. To address this issue, the laser hole-boring scheme was initially proposed [4]. This approach uses a precursor pulse to create a plasma channel that allows the main pulse to reach the core [7, 8]. However, due to filamentation instabilities [9], various suppression mechanisms [10], and other factors, the energy coupling efficiency of the hole-boring approach has been less than satisfactory. Additionally, Kodama et al. proposed another scheme with a gold cone inserted into the DT pellet [11]. In this scheme, the picosecond laser beams are injected into the gold cone, generating REB at the cone tip deep in the fuel [11, 12]. Early experiments carried out at Gekko XII laser facility [13] reported a more than 20% heating efficiency. However, subsequent studies [14–17] presented lower efficiency. More seriously, the gold cone may be deformed or damaged, before the arrival of picosecond laser beams, by the strong shocks from the imploded DT plasma [18, 19].

Recently, the double-cone ignition (DCI) scheme [20], which averts the risk of cone breaking, was proposed, as shown in Fig. 1(a). Two DT fuel shells are separately embedded in two head-on gold cones. Under the confinement and guidance of the cones, the shells are compressed and accelerated by carefully tailored nanosecond laser pulses to eject from the cone-tips and finally collide head-to-head. Because of the confinement of the compression cones, the corona of the plasma jets is peeled off, forming a concentrically pre-heated plasma in isochoric distribution with sharp ends to the REB injection. Due to the insulation of the guiding cone, the heating cone for ignition is maintained out of exposure to the high pressure plasma during the compression. When the two ejected plasma jets collide head-to-head, the density edge in the perpendicular direction is significantly sharp, features a shorter scale length to the core and provides a secure region for heating cone with reduced risk of being damaged before the REB is generated [21]. This allows for efficient injection of the REB into ~ 300 g/cm^3 high density region.

In previous studies on the transport of REB, electromagnetic (EB) field was regarded as crucial to the quality of REB, and received considerable attention [6, 22].

* dwu.phys@sjtu.edu.cn
† jzhang@iphy.ac.cn

10.1017/hpl.2025.20
https://doi.org/10.1017/hpl.2025.20 Published online by Cambridge University Press

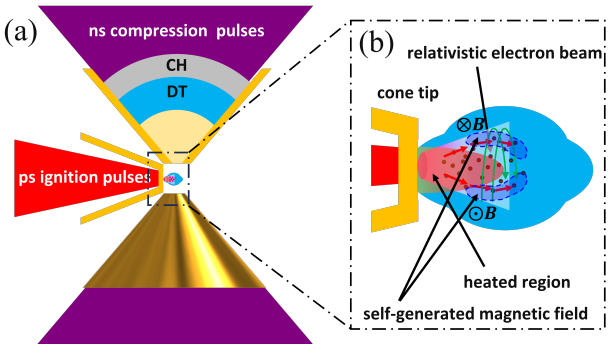

FIG. 1. (color online). (a) Schematic of DCI scheme. (b) Detailed schematic for the structure of the colliding target and the transport of fast electrons in the REB.

Taking advantage of the self-generated EB fields [23, 24], composite materials with gradient of resistivity were explored [24–27], to reduce the divergence of REB. Special configurations of cone tip were also proposed [28–31]. In the above researches, the density of plasma is relatively low, where the Ohmic effect dominates the interaction between the REB and plasma. In the configuration of simulations [32–34], for the sake of preservation of the cone tip, the REB sources are always set ~ 100 μm away from the most dense core, with the density of plasma gradually raising from several g/cm^3 to about 500 g/cm^3, and the effect of self-generated EB fields mainly reflects in this transit region.

By contrast, in the DCI scheme, the REB is directly injected into the high density core. In such regime, the collision effect between the REB and the background electrons is extremely significant. Moreover, as the DT fuel is heated up to thousands of electronvolts within several picoseconds, the DT fuel was usually modeled as ideal plasma with a low Spitzer resistivity. Therefore, the effect of EB field in the high density fuel was used to be ignored for granted. However, through our indepth investigation, self-generated EB fields indeed play important roles, which are significantly enhanced by the quantum degeneracy effects.

In this paper, we conducted rigorous theoretical analyses and unprecedented simulations to investigate the transport of the REB in high density, degenerate DT plasmas. Focusing on the transport of the REB, we model the colliding plasma as a uniform density region for simplicity, and the REB is directedly injected in to the plasma. Theoretical finding demonstrates that due to influences of quantum degeneracy, where resistivity increases with rising temperature, there exist a rapid growth of the magnetic field as the REB is injected. Furthermore, we figured out the threshold for the occurrence of the self-organized pinching of REB by the EB field. Via fully three dimensional hybrid-PIC simulations, we observed an enhancement of the heating efficiency of REB than previous intuitive expectation, as a result of the self-generated EB field in the high density quantum degenerate plasma.

This paper is organized as follows. Section II theoretically derives the growth of self-generated magnetic field, and analyses the occurrence of the self-organized pinching. Section III presents the 3D hybrid-PIC simulation results with a broad-spectrum diverging REB. Section IV quantitatively compares the deposit efficiency of the REB between EB and noEB cases, as well as the enhancement on the heating of DT plasma. In Section V our conclusions are presented.

II. THEORETICAL ANALYSIS OF SELF-GENERATED MAGNETIC FIELD FOR THE HIGH DENSITY REGIME

A. Growth rate of self-generated magnetic field in dense, collision-dominated plasma

When an REB with the current density of $\boldsymbol{j}_f$ is injected into the DT plasma along z axis, the macroscopic electrical neutrality condition should be fulfilled, leading to the drifting of background particles. Since the DT ions have a mass thousands of times larger than the mass of electrons, the drifting of background ions by the interaction with the REB is relatively negligible, and the drifting current of background electrons is $\boldsymbol{j}_b = -\boldsymbol{j}_f$. Since the thermal drift motion of the background electrons is much slower than the injected relativistic electrons ($v_e/v_f \sim 10^{-4}$), the $-\boldsymbol{v}_e \times \boldsymbol{B}$ and $-\nabla P_e/en_e$ term in the generalized Ohmic law are neglected, and an approximation of electric field of $\boldsymbol{E} = \eta \boldsymbol{j}_b$ is presented, where η is the resistivity of the background electrons. In practical case, $\boldsymbol{j}_f$ of the injected REB is spatially nonuniform, and according to Faraday's law, a magnetic field is generated with a growth of $\partial \boldsymbol{B}/\partial t = -\boldsymbol{\nabla} \times (\eta \boldsymbol{j}_b) = \boldsymbol{\nabla} \times (\eta \boldsymbol{j}_f)$. For a cylindrically symmetrical REB, neglecting the microscopic perturbations, the plasma is also assumed to be heated up symmetrically. Therefore, by noting $|\boldsymbol{j}_f|$ as $j(r)$ and η as $\eta(r)$, the azimuthal derivation $\partial/\partial\theta$ vanishes. For simplicity, we assume that $\boldsymbol{j}_f$ is only along z axis with a gradient along r axis. Under these assumptions, the growth rate of the azimuthal magnetic field can be expressed as

$$\frac{\partial B_\theta}{\partial t} = -\frac{\partial}{\partial r}(\eta j) = -\left(\eta \frac{\partial j}{\partial r} + j \frac{\mathrm{d}\eta}{\mathrm{d}T}\frac{\partial T}{\partial r}\right). \qquad (1)$$

According to Eq. (1), the growth of the magnetic field is closely dependent on the competition between η and $j(\mathrm{d}\eta/\mathrm{d}T)(\partial T/\partial r)$, assuming that the background ions and electrons are in thermal equilibrium with the same T. For the first term, the power law of $\eta \propto T^\alpha$ is applied, according to the degenerate limit of Lee-More model and the classical Spitzer model, with $\alpha = 1$ and $-3/2$ respectively representing the degenerate and classical state. For the second term, $\partial T/\partial r$ is determined by the heating efficiency,

https://doi.org/10.1017/hpl.2025.20 Published online by Cambridge University Press

$$c_v \frac{\partial T}{\partial t} = P_{\text{heat}}(j) = -\frac{j}{e}\frac{\mathrm{d}E_k}{\mathrm{d}z}, \tag{2}$$

where c_v is the heat capacity of background plasma, and P_{heat} is the heating power of REB, related to the beam current density j and the stopping power $\mathrm{d}E_k/\mathrm{d}z$. In this way, $\partial T/\partial r$ is connected to $\partial j/\partial r$. A more intensive heating current density leads to the elevation of local temperature, inducing a gradient in T with the same direction of j.

Detailed analysis of the stopping power $\mathrm{d}E_k/\mathrm{d}z$ in Appendix A demonstrates that for the REB with the intensity of 10^{20} W/cm^2 in the 300 g/cm^3 DT plasma, the collisional component in the stopping power is dominant. For the sake of simplicity and clarity in analytical derivation, the Ohmic component in Eq. (A1) is omitted in the calculation, focusing on the fundamental physics of the collisional cases. In this way, ignoring the minute changes of $\ln\Lambda_f$, the stopping power $\mathrm{d}E_k/\mathrm{d}z$ is independent of T, and hence Eq. (2) is promptly simplified into a concise form $T = T_0 + jt/C$, where T_0 is the initial temperature and C is approximately regarded as a constant. In this way, $\partial T/\partial r$ equals to $(t/C)(\partial j/\partial r)$. Let $\eta_0 = \eta(T_0)$, the growth rate of the magnetic field is calculated as

$$\frac{\partial B_\theta}{\partial t} = -\frac{\partial j}{\partial r}\eta_0 \left(1 + \frac{jt}{CT_0}\right)^{\alpha-1}\left[1 + (\alpha+1)\frac{jt}{CT_0}\right]. \tag{3}$$

The effect of quantum degeneracy is important for the growth of magnetic field. According to Eq. 1, The growth of the self-generated magnetic field is related to both η and j. During the heating process, the temperature in the center region with the highest intensity of the REB undergoes more rapid increase. Therefore, in the degenerate plasma, $\eta \propto T$ also holds its peak value in the center region, with the same trend of gradient with j, and the growth of magnetic field is consequently promoted. By substituting $\alpha = 1$ into Eq. (3), the growth of magnetic field in the degenerate turns to

$$\frac{\partial B_\theta}{\partial t} = -\frac{\partial j}{\partial r}\eta_0 \left(1 + 2\frac{jt}{CT_0}\right), \tag{4}$$

which means that $\partial B_\theta/\partial t$ is linear with respect to t, indicating a quadratic growth of magnetic field.

As for the classical $\eta \propto T^{-3/2}$ case, the two terms in the RHS of Eq. 1 possess different signs, and the growth of B_θ depends on the competition between η and $T(\mathrm{d}\eta/\mathrm{d}T)$. Numerically, Eq. (3) turns to

$$\frac{\partial B_\theta}{\partial t} = -\frac{\partial j}{\partial r}\eta_0 \left(1 + \frac{jt}{CT_0}\right)^{-5/2}\left(1 - \frac{jt}{2CT_0}\right). \tag{5}$$

When $jt/2CT_0 > 1$, it is observed from Eq. (5) that the sign of $\partial B_\theta/\partial t$ is reversed. Though, the $(1+jt/CT_0)^{-5/2}$ term decreases towards zero quickly in power of $-5/2$, which retards the decline of B_θ.

B. Numerical calculation of the self-generated magnetic field

In this section, a numerical calculation with practical parameters is presented, following the theoretical analysis in the previous section.

Firstly, a proper expression of η is particularly discussed. In many researches, to avoid the divergence of Spitzer model in the cool region, a constant scale value η_c was introduced by $\eta^{-1} = \eta_{Sp}^{-1} + \eta_c^{-1}$ [35, 36]. However, this approach eliminates the gradient of η with respect to T in the degenerate regime. In this investigation, to align with Lee's model [37], with $\alpha = 1$ for degenerated cases and $\alpha = -3/2$ for classical cases, a piece-wise approximation of η is applied as Eq. (B1), as is shown in Appendix B.

In the pursuit of rigor, this study has considered the influence of degeneracy effects on the heat capacity c_v. As is commonly known, c_v in Eq. (2) consists of the ion and the electron heat capacity. Both heat capacity equal to classical value $(3/2)n$ in classical case, where $n = n_i = n_e$ is the number density of ions or electrons for fully ionized fuel. In the strongly degenerate state, however, the heat capacity is calculated by $c_v = n(3/2 + \mathrm{d}\bar{\varepsilon}_e/\mathrm{d}T)$, where $\bar{\varepsilon}_e = \int \varepsilon f(\varepsilon)\mathrm{d}\varepsilon$ is the average energy of the background electrons, and $f(\varepsilon)$ is the Fermi-Dirac distribution.

Now all the pre-works have been done, and we numerically solve Eq. (1). After deriving Eq. (3), with the symbolic constant C being calculated along with Eq. (A1) and (B1), T is then determined as a function of t and j. Subsequently, this time-varying T is substituted back into Eq. (B1) to calculate η at specific moment, as well as its derivative to temperature $\mathrm{d}\eta/\mathrm{d}T$. By incorporating η, $\mathrm{d}\eta/\mathrm{d}T$ and $\partial T/\partial r$ into Eq. (1) and integrating both side over time, the magnetic field B_θ is finally solved.

A specific model is constructed for analysis, which refers to typical parameters for ignition [20, 38–40]. The density of the DT plasma is chosen as a representative value of 300 g/cm^3, with the Fermi temperature to be $T_F = 629.17$ eV. The beam number density follows a bell-shaped distribution $n_f(r) = n_f(0)\exp(-r^2/\sigma^2)$ along r axis, with a peak value of $n_f(0) = 2.5\times10^{22}$ cm^{-3} and a waist of $\sigma = 20\mu$m. Consequently, the current density is in form of $j(r) \approx n_f(0)ec\exp\left(-r^2/\sigma^2\right)$. For the simplicity of calculating the current density j, we assume an idealized exponent kinetic energy spectrum $f(E) \propto \exp(-E/E_{k_0})$ for the REB, with $E_{k_0} = 1.5$ MeV, and the corresponding beam intensity integrating over the energy spectrum E is $I(0) \approx n_f(0)E_{k_0}c = 2\times10^{20}$ W/cm^2. The profile of j is assumed to be invariant, while the lateral movement will be discussed in the following.

According to Eq. (3), the growth rate $\partial B_\theta/\partial t$ is self-similar in scale of jt/CT_0, and Fig. 2 shows a typical calculation of B_θ and T at $r = \sigma$. In high density regime, the primary contribution to heating the DT fuel is the collision effect between the fast electrons and background electrons, and T is raised near-linearly. The green and yellow region in Fig. 2 roughly separate the degenerate

https://doi.org/10.1017/hpl.2025.20 Published online by Cambridge University Press

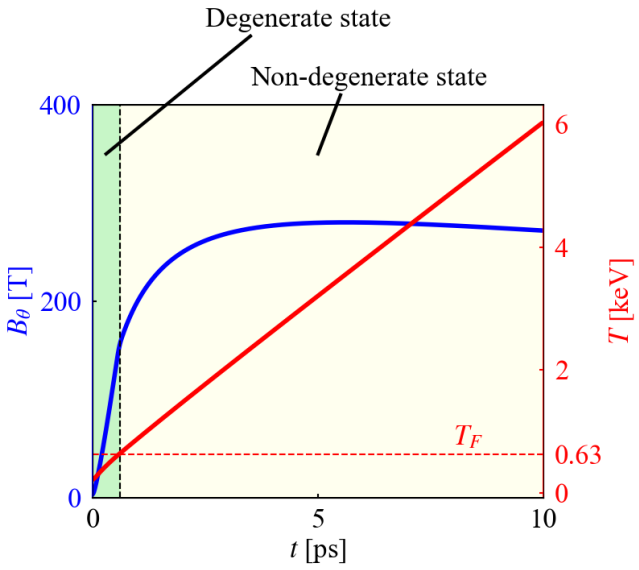

FIG. 2. (color online). Theoretical calculation of B_θ and T at the position of $r = \sigma$, for a bell-shaped REB with $I(0) = 2 \times 10^{20}$ W/cm^2 in 300 g/cm^3, $T_0 = 200$ eV DT plasma. The green and yellow background color indicates the degenerate and non-degenerate state.

and non-degenerate states by the Fermi temperature T_F. Notably, though the degenerate state last for merely a short time less than 1 ps compared with the ~ 10 ps full fast heating process, the quadratic growth of B_θ in the early degenerate stage is quite crucial. As the plasma is heated up and turns non-degenerate, the growth of B_θ is decreasing as expected. However, the already generated B_θ in the initial degenerate stage still sustains for a long while, and leads to self-organized pinching of the REB.

C. Threshold for the self-organized pinching

In the practical fast heating process, attention should be attached to the self-organized pinching of the REB. Due to the degenerate effect, the self-generated EB field rises rapidly to deflect and concentrate the REB. Consequently, the current density j increases while the waist of the REB decreases, and hence $\partial j/\partial r$ in Eq. (3) rises, accelerating the growth of the magnetic field. In turn, the boosted magnetic field further pinches the diverging fast electrons towards the center. It should be clarified that the ~ 10 ps time span of fast heating is insufficient for hydrodynamic effects of the background plasma to occur, therefore this self-organized pinching is purely electromagnetic in nature.

To determine the threshold at which the magnetic field will inevitably evolve into the pinching process, we outline an estimation of the required magnetic fields, in which the Larmor radius of fast electrons is of key roles, $r_L = \gamma m_e v/eB$, where γ is the Lorentz factor of the electron and v is the corresponding velocity. For an REB out of the guiding gold cone tip, its divergence is model as a Gaussian function $f(\theta) \propto \exp(-\theta^2/\theta_0^2)$ characterized by θ_0 [6, 41]. It is essential that the transverse extension of the magnetic field along r direction, denoted as L, should be at least equivalent to $r_L(1 - \cos\theta_0)$ at a particular instant. Once the equation

$$\int_0^L B_\theta(r)dr > \gamma \frac{m_e v}{e}(1 - \cos\theta_0) \text{ for pinching} \qquad (6)$$

is fulfilled, most of the diverging electrons are deflected by the EB field, causing them to converge towards the beam center. For a rough estimation, substituting $L = 10$ μm, $\theta_0 = 30°$ and $\gamma = 3.9$ (corresponding to 1.5 MeV) into Eq. (6), a 10 μm scale of magnetic field with $B > 90$ T is required, which is available under the parameter of theoretical calculation.

III. RESULTS OF 3D HYBRID-PIC SIMULATIONS ON THE TRANSPORT OF THE BRAOD-SPECTRUM DIVERGING REB

A. Introduction of LAPINS code and simulation settings

To examine the theoretical analysis, we conducted 3D3V hybrid-PIC simulations with the LAPINS code [42–45]. LAPINS is a hybrid-PIC code compatible with simulation of degenerate and dense plasmas over large scale by improving interactions of collision and electromagnetic field. Compared with conventional PIC codes, LAPINS modifies the kinetic equation to Boltzmann-Uhling-Uhlenbeck equations, where the Pauli exclusion principle is considered in collision term. With this approach [44], Fermi-Dirac statistics are implemented to degenerate particles. Different from other hybrid-PIC codes, in LAPINS code, hydro method is only applied to solve the electromagnetic field, while the background electrons and ions are still treated as discrete particles. Hence, the collisions between ions, background electrons and injected electrons are self-consistently included through the Monte-Carlo schemes [46–48]. Benchmarks for the correctness of collision module and range of fast electrons are presented in Appendix C.

The major configurations for simulation are listed as follow, referring to [20, 38–40]. Due to the special sharp density edge in the DCI scheme, we assume that the REB is directly injected into the high density isochoric plasma in our simulations. The density of DT plasma is 300 g/cm^3, corresponding to a number density of $n_e = n_i = 7.2 \times 10^{25}$ cm^{-3}, and the initial temperature is $T_0 = 200$ eV. The REB is injected into the 300 g/cm^3, 200 eV degenerate DT plasma. A complete distribution of the broad spectrum, diverging and bell-shaped REB is written as

https://doi.org/10.1017/hpl.2025.20 Published online by Cambridge University Press

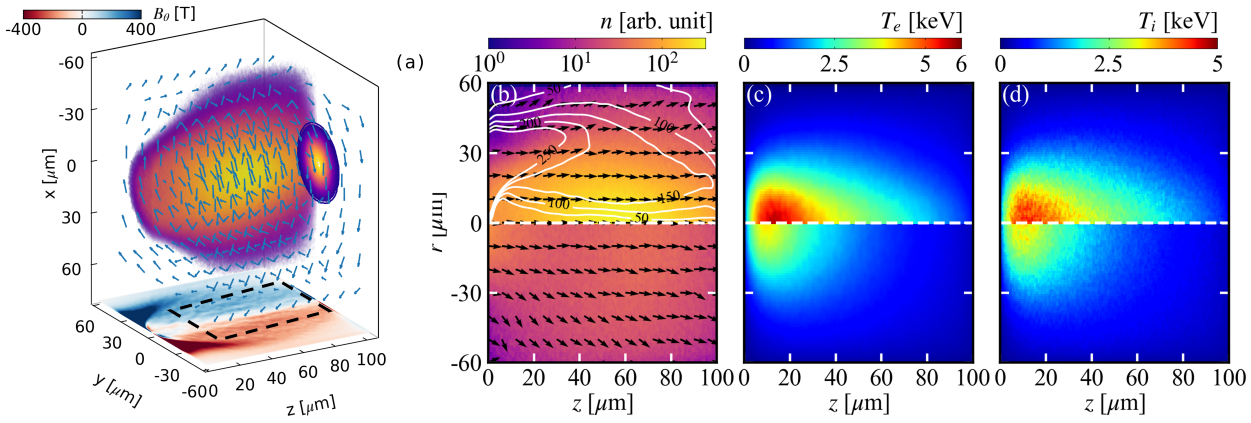

FIG. 3. (color online). Snapshots of the transport of REB in DT plasma at $t = 10$ ps. (a) Deposition of injected electrons, vector schematic of self-generated magnetic field and profile of B_θ. (b-d) Profile of the distribution of deposited, injected electrons, electron temperature and ion temperature at $x = 0$. For comparison, the bottom half part of (b-d) shows the noEB simulation result, which turns off the EB field. To demonstrate the pinching of the self-generated EB field, the contours in (b) indicates the intensity distribution of the magnetic field B_θ, and the black quivers indicate the direction of REB's current density $-\boldsymbol{j}_f/|j|$.

$$n_f(r, E_k, \theta) \propto 2\pi r \exp\left(-\frac{r^2}{\sigma^2}\right) \exp\left(-\frac{|E_k - 1.5\ \text{MeV}|}{1\ \text{MeV}}\right) \exp\left(-\frac{\theta^2}{\theta_0^2}\right), \tag{7}$$

where $\sigma = 20$ μm and $\theta_0 = 30°$. The total energy carried by the REB injected into the system is 40 kJ, and the injection power is constant in the 10 ps simulation span. The fast electrons are real particles injected into the system at each time step, randomly assigned the r-position, kinetic energy and momentum according to Eq. (7) and the total energy requirement. Therefore, the transport and stagnation process of the injected electrons is self-consistent.

The size of simulation region is 120 μm × 120 μm × 100 μm with Cartesian coordinates, with the length of each meshgrid to be 1 μm along x and y axis, and 0.5 μm along z axis. The fields adhere to the periodic boundary condition, and the background ions and electrons adhere to the thermal boundary condition. Particularly, the injected electrons apply the absorbing boundary. The time step dt is set to be 1.67 fs. The DT ions are equivalent to a virtual species of particle with a mass number of $A = 2.5$, and the nuclear fusion module is turned off. The particle per cell (ppc) of background ions and electrons are both 64. The REB is injected at $z = 0$ from the left boundary of the simulation region. In each time step, the ppc of fast electrons generated in the boundary cell is 8. To ensure the computation efficiency, an upper limit of 400 is imposed on the ppc of fast electrons. A newly developed merging algorithm [49] is applied to the injected electrons, which simultaneously ensures the conservation of energy, momentum, and current density, while decreases the number of virtual particles to achieve greater computing speed.

B. Simulation results

The simulation results are presented in Fig. 3. As shown in Fig. 3(a), significant self-generated EB fields are generated in the high density plasma. Clear illustration of the temporal evolution of the magnetic field profile is presented in Fig. 4(a-d). The B_θ exhibits a significant trend of pinching towards the center like a pair of folded wings, with the field intensity in the "mid-wing" region exceeding 200 T. The extraordinarily large field intensity near the injection edge $z = 0$ results from the overly idealized REB shape, whereas in reality the stacking and transverse spread of low energy electrons would lessening the field. Hence, to focus on the self-organized pinching and to check with theoretical calculation, maximum value of B_θ is only collected with the region of $z > 20$ μm and $r < 30$ μm, as is marked by the black dotted box in Fig. 3(a).

The growth line of maximum B_θ is illustrated in Fig. 5(a). Due to the divergence of the REB, the equivalent current density along z axis is lower than that in the 1D theoretical calculation. However, the simulation results match the theoretical trend well. In the first 1 ps, when the peak temperature of background electrons is still lower than 1 keV and most of the system is in state of degenerate, B_θ rises quadratically consis-

https://doi.org/10.1017/hpl.2025.20 Published online by Cambridge University Press

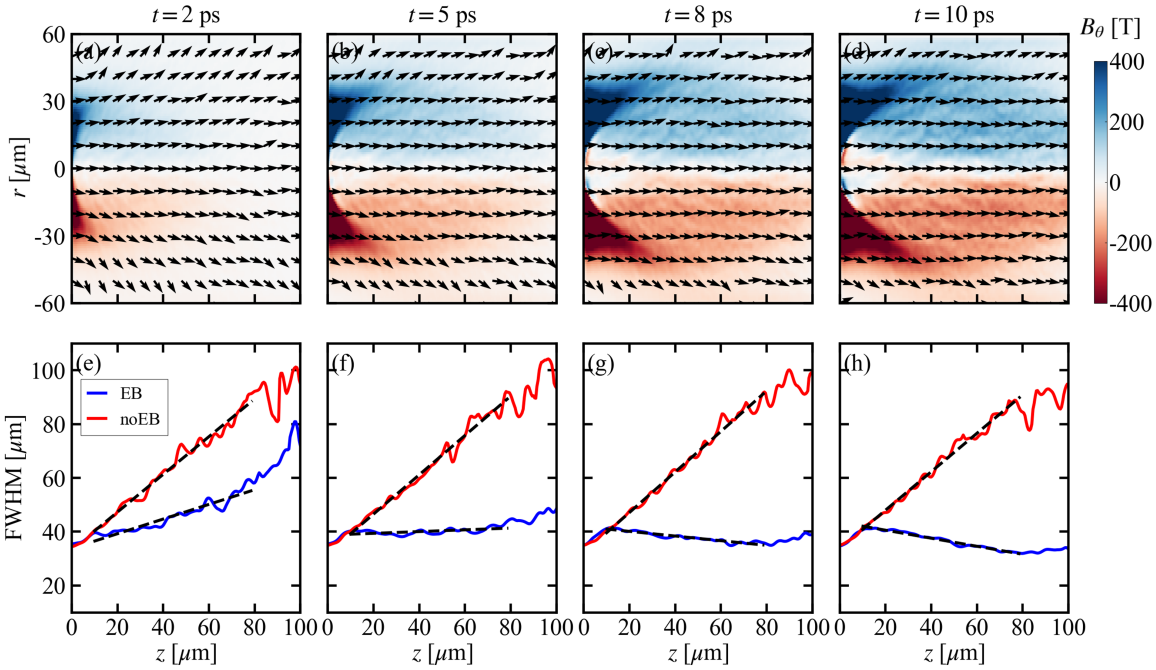

FIG. 4. (color online). (a-d) Snapshots of the self-generated magnetic field B_θ at $t = 2$ ps, 5 ps, 8 ps and 10 ps in the EB case. The black arrows show the direction of REB's current density $-\boldsymbol{j}_f/|j|$. (e-h) the FWHM of REB's current density j along z axis at the corresponding moment. The black dotted lines indicate the linear fitting result, with the slopes shown in Table I.

TABLE I. Linear fitting slope d(FWHM$_{|j|}$)/dz according to Fig. 4(e-h). The region for least square fitting from $z = 10$ μm to $z = 80$ μm.

	$t = 2$ ps	$t = 5$ ps	$t = 8$ ps	$t = 10$ ps
EB	0.26	0.03	-0.08	-0.15
noEB	0.59	0.67	0.67	0.61

tent with the prediction of Eq. (3), and a considerable magnetic field of about 100 T is generated just in this instant. Then, the growth of B_θ goes over the inflection point and slows down, as the plasma is heated up and becomes non-degenerated. Up to $t = 5$ ps, the line of B_θ in Fig. 5(a) shows a high degree of similarity with $r = \sigma$ line in Fig. 2(b). However, as the magnetic field increases strong enough to deflect diverging electrons to the center, the self-organized pinching effect occurs to concentrate the REB, leading to an boosted increase in the EB field, with B_θ rising from 150 T to nearly 250 T in the subsequent 5 ps of the heating process.

This magnetic field effectively concentrates the deposition of injected electrons. The top half of Fig. 3(b), representing the EB case, shows a significantly denser deposition compared to the bottom half, which represents the noEB case. The black arrows in Fig. 3(b) represent the unit vector $-\hat{\boldsymbol{j}}_f = -\boldsymbol{j}_f/|j|$, indicating the flow direction of the REB. It is noted that in the top half the arrows predominantly point forward due to the collimating effect of the self-generated EB field, whereas in the bottom half, the arrows diverge as initially configured. The direction of REB's current density $-\hat{\boldsymbol{j}}_f$ in the EB case is also plotted in Fig. 4(a-d). At $t = 2$ ps, $-\hat{\boldsymbol{j}}_f$ shows the typical divergence of REB, as in the initial settings. However, as the magnetic field B_θ grows over 100 T at $t = 5$ ps, the diverging trend is restrained, and $-\hat{\boldsymbol{j}}_f$ is gradually collimated to the beam center. When the simulation duration exceeds 8 ps, most of the $-\hat{\boldsymbol{j}}_f$ arrows has pointed forward along z axis.

The divergence of the REB can be characterized by the profile of current density $|j|$ along z axis. To attain the multiple relationship clearly, $|j|$ is normalized by the maximum of the counted profiles. As is shown in Fig. 5(c), $|j|$ has a broader profile in the noEB case, and decreases rapidly as z increases deeper into the plasma, which indicates that the injected electrons have been scattered and the REB is diverging. In contrast, due to the pinching of the self-generated EB field, the REB in the EB case still remains a considerable intensity even

https://doi.org/10.1017/hpl.2025.20 Published online by Cambridge University Press

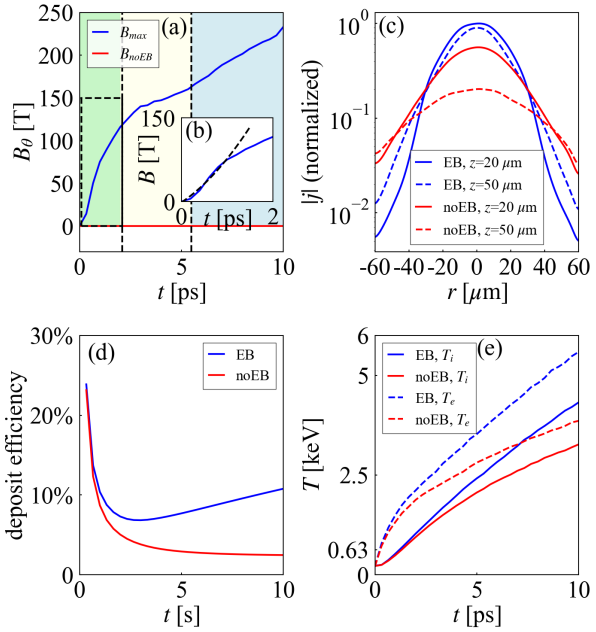

FIG. 5. (color online). (a) Maximum value of B_θ within the statistical region shown in Fig. 3(a). The stages of degenerate state, non-degenerate state and pinching are indicated by the green, yellow and blue background color. (b) The detailed profile of $B_{\max}$ in the first 2 ps and the corresponding quadratic fitting line (the black dotted line). (c) Profile of $|j|$ at $t = 10$ ps in EB and noEB simulations along r axis, normalized by the maximum value of the blue solid line. (d) Deposit efficiency of the REB in EB and noEB simulations. (e) Maximum value of T_i and T_e of plasma in EB and noEB simulations.

after transporting deeply to $z = 50$ μm, and the waist expansion is minimal. In comprehensive consideration, the divergence of the REB during transport is quantified by $\mathrm{d}(\mathrm{FWHM}_{|j|})/\mathrm{d}z$, obtained through a least-squares fit from $z = 10$ μm to 80 μm, as is shown in Fig. 4(e-f). Due to the diverging angle θ_0 in the initial settings and the collisional scattering, as is shown by the red lines in the noEB case, $\mathrm{FWHM}_{|j|}$ is broadening as z increases. However, when considering the effect of EB field, the profile of $\mathrm{FWHM}_{|j|}$ changes significantly. Even at $t = 2$ ps in Fig. 4(e), the blue line of EB case exhibits a slower growth rate than the red line, which indicates a smaller diverging angle. At $t = 5$ ps, $\mathrm{FWHM}_{|j|}$ in the EB case no longer increases over z, and the REB has been collimated. As for t exceeding 8 ps, the slope $\mathrm{d}(\mathrm{FWHM}_{|j|})/\mathrm{d}z$ turns negative, which means that the waist of the REB is shrinking over z, and the REB is pinched by the self-generated magnetic field.

C. Analysis of the deposit efficiency of the REB and enhancement of the fast heating

The pinching of the REB significantly impacts the deposit of injected electrons. Fig. 5(d) illustrated the deposit efficiency of the REB, which is defined as the ratio of the number of the injected electrons deposited in the heating region, to the number of the total injected electrons in the REB. A high deposit efficiency indicates that more injected electrons deposit their energy in a localized region, making a most usage of the energy of the REB. According to the profile of electron and ion temperature shown in Fig. 3(c) and (d), The heating region of the DT plasma has been estimated as a cylinder, with the lateral radius $r = \sqrt{x^2 + y^2}$ less than 20 μm. It can be noted in Fig. 5(d) that in both simulations, the deposit efficiency decreases over time in the beginning stage. However, the blue line representing the EB case increase after $t = 3.5$ ps, which means that more injected electrons are concentrated to the heating region by the great EB field and pinching. At $t = 10$ ps, the deposit efficiency is merely 2.46% for the noEB case, while 10.78% for the EB case, showing a significant difference larger than 8%. Accordingly, the pinching is promotive for the concentrated deposit of the REB, to form a localized hot spot for ignition.

To directly demonstrates the effect of pinching on the ignition, the electron and ion temperature of the DT plasma is also discussed. The top half of Fig. 3(c) and (d), representing the EB case, shows a larger and hotter heated region, which extends deeper along the z axis. The increase of the maximum value of T_e and T_i are shown in Fig. 5(e). It can be observed that T_i is always lower than T_e, since the heating of DT ion is through the relaxation with bulk electrons. A temperature difference between the EB and noEB cases emerges after 1 ps, when the field has grown beyond 100 T and begins to concentrate injected electrons. As the pinching effect intensifies, the temperature gap finally rises to 1 keV at $t = 10$ ps, when T_i in the EB case has reached 4.3 keV. To save computational resources, the nuclear reaction module is not included in simulations. If considering additional fusion α-particle heating from burn of the DT fuel, the sensitively T-dependent fusion reactivity in the EB case is nearly two order of magnitude by that in the noEB case [50], and the gap of T_i between EB and noEB cases will be far more remarkable. It is expected that the entire heated region in the EB case would exceed 5 keV, forming a hot spot for ignition. Using the same estimation of the heating region as the last paragraph, and defining the heating efficiency as the increase of DT ion internal energy in the heated region divided by the energy total injected by the REB, the heating efficiency is 11.69% in the noEB case and rises to 19.75% in the EB case, which comes out nearly a two-fold increase. This result indicates that the effect of pinching and self-generated EB field in the high density plasma has been significantly underestimated in the previous studies.

https://doi.org/10.1017/hpl.2025.20 Published online by Cambridge University Press

IV. DISCUSSION AND CONCLULSIONS

During the transport of fast heating with REB directly injected into the dense and degenerate ($n_e \sim 10^{25}$ cm^{-3}, $T \sim 100$ eV) plasma generated by the colliding of high speed plasma jets from two gold cones, we particularly investigate and reveal the significant effect of quantum degeneracy on the rapid growth of self-generated EB field and the trigger of the self organized pinching, which were neglected by previous works for granted. Due to the favorable spatial configuration of resistivity in state of degeneracy, the self-generated EB field grows rapidly in the initial stage, and further promotes the concentration of the REB to deposit energy in a limited region. Enhancement on the deposition efficiency of the injected electrons has been observed in the 3D hybrid-PIC simulation, and this consequently results in a two-fold heating effect for ignition. Additionally, in the researches on the ultra-intense laser-solid interactions, energetic electron bunches are driven through the strongly degenerate solid material or warm dense matter. Hence, the self-organized pinching is also intricately linked to vast topics of ultra-intense laser based applications, encompassing laser-driven ion acceleration [51, 52], neutron sources [53], THz radiation [54, 55] and the creation of transient warm dense matter.

Based on this investigation, further perspective is proposed for practical implementations. To take advantage of the degeneracy, employing a non-exponential energy distribution on the REB, with a reduced proportion of low-energy electrons, is advantageous for fostering the pinching, since this approach prevents excessive heating of the plasma near the injection position. Moreover, synergistic effect of exerted assisting magnetic field [56] along z axis and self-generated EB field is also worthwhile to investigate in the future.

There are still some limitations in this investigation. To simulate large-scale, high-density plasma while accounting for both binary collisions and electromagnetic fields, we employed a hybrid-PIC algorithm [44]. However, this approach may overlook microscopic kinetic perturbations, such as filamentation of the REB. The idealized REB model used in the simulation causes a strong magnetic field near the injection edge, which is not supposed to occur in reality. Additionally, we applied a piecewise resistivity model in our theoretical analysis to qualitatively describe the quantum degeneracy effect and the self organized pinching, while the resulting B_θ may quantitatively change as a more accurate description of resistivity is used.

Experimental validation is planned at the Shenguang II laser facility, where integrated experiments of the DCI scheme is conducted. Three electron spectrometers are planned to be positioned at different angles to the transport direction of the REB, to get the angular distribution of the escaping fast electrons passing through the dense plasma, which may provide valuable insights into the role of EB field and quantum degeneracy in enhancing the heating efficiency of REB.

This work is supported by the Strategic Priority Research Program of Chinese Academy of Sciences (Grant Nos. XDA25010100 and XDA25050500), National Natural Science Foundation of China (Grants No. 12075204), and Shanghai Municipal Science and Technology Key Project (No. 22JC1401500). Dong Wu thanks the sponsorship from Yangyang Development Fund.

Appendix A: Analysis of Ohmic and collisional stopping power for high density plasma

In this section a theoretical analysis of stopping power $\mathrm{d}E_k/\mathrm{d}z$ for the transport of REB in the high density DT plasma is conducted. Referring from [36], in which a comprehensive stopping power model is displayed,

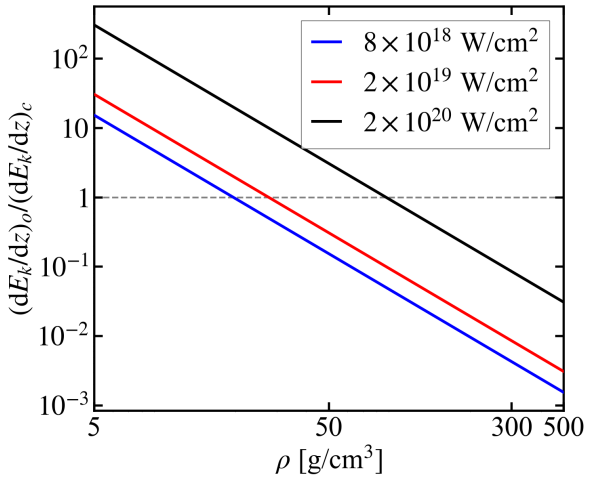

FIG. 6. (color online). Ratio of the Ohmic component $(\mathrm{d}E_k/\mathrm{d}z)_o$ to the collision component $(\mathrm{d}E_k/\mathrm{d}z)_c$ as a function of background DT plasma's density ρ (g/cc), under the corresponding Fermi temperature of each certain ρ. The blue, red and black solid lines represent the calculation results with the intensity of the REB I equal to 8×10^{18} W/cm^2, 2×10^{19} W/cm^2 and 2×10^{20} W/cm^2, respectively.

$$\frac{\mathrm{d}E_k}{\mathrm{d}z} = \left(\frac{\mathrm{d}E_k}{\mathrm{d}z}\right)_c + \left(\frac{\mathrm{d}E_k}{\mathrm{d}z}\right)_o = -\frac{4\pi e^4 n_b}{m_e c^2}\Gamma(E_k)\ln\Lambda_f - \eta e^2 n_f c \frac{1}{\sqrt{\Gamma(E_k)}}. \quad \text{(A1)}$$

In Eq. (A1), the Ohmic component $(\mathrm{d}E_k/\mathrm{d}z)_o$ represents the deceleration effect of the electric field of return current [23]. The electric field equals to resistivity times current density, $\boldsymbol{E} = \eta \boldsymbol{j}_b = -\eta \boldsymbol{j}_f$, is generated to decelerate fast electrons, where η is the resistivity of the background electrons. Let $j = |\boldsymbol{j}_f|$, and the Ohmic component is written as $(\mathrm{d}E_k/\mathrm{d}z)_o = e\eta j$.

https://doi.org/10.1017/hpl.2025.20 Published online by Cambridge University Press

Meanwhile, the injected fast electrons collide with background electrons [57], also transforming directional kinetic energy into disordered thermal energy, which corresponds to the collisional component $(\mathrm{d}E_k/\mathrm{d}z)_c = \kappa_0 n_i[Z_i \ln\Lambda_f + (Z - Z_i)\ln\Lambda_b]$, where Z_i and $(Z - Z_i)$ are respectively the number of free and bound electrons, $\ln\Lambda_f$ and $\ln\Lambda_b$ are respectively the Coulomb logarithms for collisions with free and bounded electrons, and $\kappa_0 = 4\pi e^4/m_e v_f^2$ is the stopping factor. For fully ionized DT plasma $Z_i = 1$ and $(Z - Z_i) = 0$.

In FI scheme, fast electrons have an energy of $E_k \sim$ MeV, therefore v_f approximates to c, and a relativistic relationship $v_f = c/\Gamma(E_k)$ is added to stopping power, where $\Gamma(E_k) = \gamma^2/(\gamma^2 - 1)$ and $\gamma = 1 + E_k/m_e c^2$ is the Lorentz factor.

In the high density regime of $\rho \sim 100$ g/cc, the collisional component $(\mathrm{d}E_k/\mathrm{d}z)_c$ proportional to n_e rises significantly. However, in many previous studies [6, 22–24], merely the Ohmic component has been taken into account. To address this gap, the ratio of Ohmic component to collisional component of $E_k = 1.5$ MeV fast electrons is calculated. The number density of background electrons n_e ranges from 10^{24} cm^{-3} to 10^{26} cm^{-3}, corresponding to the density of DT plasma ρ ranges from 5 g/cc to 500 g/cc. The temperature is set to be the corresponding Fermi temperature of each density, where the resistivity is the greatest, indicating that $(\mathrm{d}E_k/\mathrm{d}z)_o$ reaches its maximum under the given density. Besides, $(\mathrm{d}E_k/\mathrm{d}z)_c \sim \ln\Lambda_f \sim \ln(\sqrt{T})$ is generally insensitive to the variation of temperature.

The calculation result is shown in Fig. 6. The intensity of REB is represented by $I \approx n_f E_k c$, since $\Gamma(E_k)$ tends to 1 in scale of $E_k \sim$ MeV. According to Fig. 6, the neglect of the collisional component is only applicable in the low density regime, for instance, when $\rho \sim 10$ g/cc, and the ratio $k = (\mathrm{d}E_k/\mathrm{d}z)_o/(\mathrm{d}E_k/\mathrm{d}z)_c$ exceeds 10^2 for an REB as intense as $I \sim 10^{20}$ W/cm^2. However, in the high density regime of plasma with $\rho > 50$ g/cc, $(\mathrm{d}E_k/\mathrm{d}z)_c$ has become comparable to $(\mathrm{d}E_k/\mathrm{d}z)_o$. Under the condition for ignition, with $\rho \sim 100$ g/cc and $I \sim 10^{20}$ W/cm^2, the ratio k falls close to 0.1, which indicates that the collisional component is nearly ten folds of Ohmic component, and dominates the stagnation of the REB.

Appendix B: Analysis on the resistivity of degenerate plasma

In order to perform a concise analytical derivation, meanwhile representing the essence of quantum degeneracy, a proper piece-wise expression of η is applied as

$$\eta = \frac{4\sqrt{2\pi} m_e^{1/2} e^2 \ln\Lambda_f}{3(T + T_F)^{3/2}} \min\{1,\ T/T_F\}, \tag{B1}$$

in which $4\sqrt{2\pi} m_e^{1/2} e^2 \ln\Lambda_f / 3T^{3/2}$ originates from the Spitzer model, with T substituted by $T + T_F$ accounting for the quantum degeneracy effect, where $T_F = (\hbar^2/2m_e)(3\pi^2 n_e)^{2/3}$ is the Fermi temperature. In this paper, the Boltzmann constant k_B is omitted, and temperature also possesses the dimension of energy. The Coulomb logarithm is defined as $\ln\Lambda_f = \max\{\ln(1 + \lambda_D/b), 2\}$, where $\lambda_D^{-2} = \sqrt{\lambda_{De}^{-2} + \lambda_{Di}^{-2}}$ is the Debye length and $b = \max\{e^2/m_e v_{th}^2,\ \hbar/m_e v_{th}\}$. The expressions for λ_{De} and λ_{Di} are given by $\lambda_{De} = \sqrt{(T + T_F)/4\pi n_e e^2}$ and $\lambda_{Di} = \sqrt{T/4\pi n_i e^2}$, respectively. For fully ionized DT plasma, the number density of ions n_i is equal to n_e. A curve for the resistivity of 300 g/cm^3 DT plasma is displayed in Fig. 7.

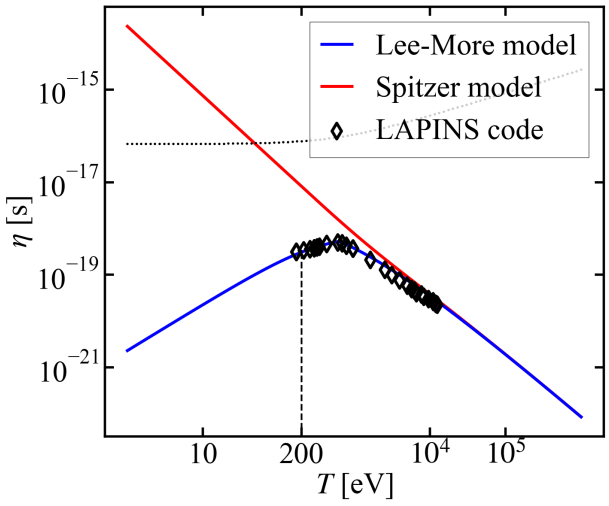

FIG. 7. (color online). Resistivity (in Gaussian unit) of 300 g/cm^3 DT plasma in the classical Spitzer model, and the Lee-More model in form of Eq. (B1). The upper limit $\eta_{\max}$ is shown in the black dotted line. The η in LAPINS code is depicted as scatters of black diamonds.

There may exist concerning on the upper limit of collision frequency $\nu_{\max}$, that the mean free path $\lambda_{mfp} = v_{th}/\nu_{\max}$ of the electrons, where $v_{th} = \sqrt{3(T + T_F)/m_e}$ is the thermal velocity, should exceed the inter-atomic distance $R_0 = (4\pi n_e/3)^{-1/3}$ [58, 59]. The upper limit of resistivity in Drude model $\eta_{\max} = m_e \nu_{\max}/e^2 n_e$ is also illustrated in Fig. 7. In the dense regime of 300 g/cm^3 for DT plasma, the expression Eq. (B1) is reasonable, always below the upper limit.

Appendix C: Benchmark of the range of fast electrons with LAPINS code

Monte Carlo method [46–48, 60] is applied in the collision algorithm, and the accuracy of collision module has been checked for simulations. The collision algorithm in LAPINS code is based on the work of Pérez et al. [48]. To validate the correctness of the theoretical analysis, a

https://doi.org/10.1017/hpl.2025.20 Published online by Cambridge University Press

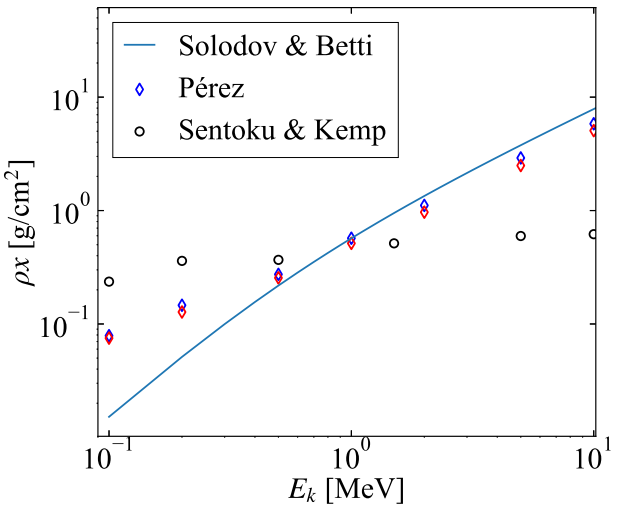

FIG. 8. (color online). Benchmark of the range of the 1.5 MeV REB in 300 g/cm^3 and 5 keV DT plasma. The blue solid line is the fitting curve given by Solodov and Betti. The diamonds represents the result of Lapins applying the algorithm of Pérez et al, with red diamonds indicating a dynamic Debye length. The black dots represents the result applying the algorithm of Sentoku and Kemp.

1D benchmark of the range of 1.5 MeV monoenergetic REB in 300 g/cm^3 and 5 keV DT plasma has been carried out. As is shown in Fig. 8, the results correspond well to the theory developed by Solodov and Betti [57]. As a supplement of the argument in [48] regarding the SK numerical algorithm [47], it is noted that the alternation between the center mass frame and the one particle at rest frame is inaccurate even on condition that one of the colliding particles is non-relativistic in the laboratory frame. This may lead to an incorrect estimation of the range of relativistic electrons, and this deviation is also observed in the open source PIC code EPOCH.

Particularly, LAPINS code employs a dynamic Coulomb logarithm $\ln\Lambda = \ln(1 + \lambda'_D/b')$ [61], with $\lambda'_D = \sqrt{(T/4\pi n_e e^2)\,[1 + (\beta^2/v_{th}^2)]}$ and $b' = \min\{e^2/m_e\beta^2,\ \hbar/m_e\beta\}$, where β is the relative velocity of two particles, and $v_{th} = \sqrt{(3T/m_e)}$ is the average thermal velocity. In slow velocity limit $v_f \ll v_{th}$, β equals to $\sqrt{2}v_{th}$, and $\ln\Lambda'_D$ reduces to the static Coulomb logarithm $\ln\Lambda_D$, differing by a negligible constant $\ln(\sqrt{3})$. In high velocity regime, the range of fast electrons with dynamic Coulomb logarithm model is lower, as is shown in Fig. 8.

[1] H. Abu-Shawareb, R. Acree, P. Adams, J. Adams, B. Addis, R. Aden, P. Adrian, B. Afeyan, M. Aggleton, L. Aghaian, and The Indirect Drive ICF Collaboration, Achievement of target gain larger than unity in an inertial fusion experiment, Physical Review Letters **132**, 065102 (2024).

[2] A. L. Kritcher, A. B. Zylstra, C. R. Weber, O. A. Hurricane, D. A. Callahan, D. S. Clark, L. Divol, D. E. Hinkel, K. Humbird, O. Jones, J. D. Lindl, S. Maclaren, D. J. Strozzi, C. V. Young, A. Allen, B. Bachmann, K. L. Baker, T. Braun, G. Brunton, D. T. Casey, T. Chapman, C. Choate, E. Dewald, J. Nicola, M. J. Edwards, S. Haan, T. Fehrenbach, M. Hohenberger, E. Kur, B. Kustowski, C. Kong, O. L. Landen, D. Larson, B. J. MacGowan, M. Marinak, M. Millot, A. Nikroo, R. Nora, A. Pak, P. K. Patel, J. E. Ralph, M. Ratledge, M. S. Rubery, D. J. Schlossberg, S. M. Sepke, M. Stadermann, T. I. Suratwala, R. Tommasini, R. Town, B. Woodworth, B. V. Wonterghem, and C. Wild, Design of the first fusion experiment to achieve target energy gain G > 1, Physical Review E **109**, 025204 (2024).

[3] J. Nuckolls, L. Wood, A. Thiessen, and G. Zimmerman, Laser compression of matter to super-high densities: Thermonuclear (ctr) applications, Nature **239**, 139 (1972).

[4] M. Tabak, J. Hammer, M. E. Glinsky, W. L. Kruer, S. C. Wilks, J. Woodworth, E. M. Campbell, M. D. Perry, and R. J. Mason, Ignition and high gain with ultrapowerful lasers, Physics of Plasmas **1**, 1626 (1994).

[5] M. Tabak, D. S. Clark, S. P. Hatchett, M. H. Key, B. F. Lasinski, R. A. Snavely, S. C. Wilks, R. P. J. Town, R. Stephens, E. M. Campbell, R. Kodama, K. Mima, K. A. Tanaka, S. Atzeni, and R. Freeman, Review of progress in fast ignition, Physics of Plasmas **12**, 10.1063/1.1871246 (2005).

[6] A. Robinson, D. Strozzi, J. Davies, L. Gremillet, J. Honrubia, T. Johzaki, R. Kingham, M. Sherlock, and A. Solodov, Theory of fast electron transport for fast ignition, Nuclear Fusion **54**, 054003 (2014).

[7] A. Pukhov and J. Meyer-ter Vehn, Laser hole boring into overdense plasma and relativistic electron currents for fast ignition of icf targets, Physical review letters **79**, 2686 (1997).

[8] Y. Sentoku, W. Kruer, M. Matsuoka, and A. Pukhov, Laser hole boring and hot electron generation in the fast ignition scheme, Fusion Science and Technology **49**, 278 (2006).

[9] K. A. Tanaka, M. M. Allen, A. Pukhov, R. Kodama, H. Fujita, Y. Kato, T. Kawasaki, Y. Kitagawa, K. Mima, N. Morio, H. Shiraga, M. Iwata, T. Miyakoshi, and T. Yamanaka, Evidence of relativistic laser beam filamentation in back-reflected images, Physical Review E **62**, 2672 (2000).

[10] P. Mulser and R. Schneider, On the inefficiency of hole boring in fast ignition, Laser and Particle Beams **22**, 157 (2004).

[11] R. Kodama, P. A. Norreys, K. Mima, A. E. Dangor, R. G. Evans, H. Fujita, Y. Kitagawa, K. Krushelnick, T. Miyakoshi, N. Miyanaga, T. Norimatsu, S. J. Rose, T. Shozaki, K. Shigemori, A. Sunahara, M. Tampo, K. A. Tanaka, Y. Toyama, T. Yamanaka, and M. Zepf, Fast heating of ultrahigh-density plasma as a step towards

https://doi.org/10.1017/hpl.2025.20 Published online by Cambridge University Press

laser fusion ignition, Nature **412**, 798 (2001).

[12] C. Stoeckl, T. R. Boehly, J. A. Delettrez, S. P. Hatchett, J. A. Frenje, V. Y. Glebov, C. K. Li, J. E. Miller, R. D. Petrasso, F. H. Séguin, V. A. Smalyuk, R. B. Stephens, W. Theobald, B. Yaakobi, and T. C. Sangster, Hydrodynamics studies of direct-drive cone-in-shell, fast-ignitor targets on omega, Physics of Plasmas **14**, 10.1063/1.2812706 (2007).

[13] R. Kodama, H. Shiraga, K. Shigemori, Y. Toyama, S. Fujioka, H. Azechi, H. Fujita, H. Habara, T. Hall, Y. Izawa, T. Jitsuno, Y. Kitagawa, K. M. Krushelnick, K. L. Lancaster, K. Mima, K. Nagai, M. Nakai, H. Nishimura, T. Norimatsu, P. A. Norreys, S. Sakabe, K. A. Tanaka, A. Youssef, M. Zepf, and T. Yamanaka, Fast heating scalable to laser fusion ignition, Nature **418**, 933 (2002).

[14] H. Azechi, K. Mima, S. Shiraga, S. Fujioka, H. Nagatomo, T. Johzaki, T. Jitsuno, M. Key, R. Kodama, M. Koga, K. Kondo, J. Kawanaka, N. Miyanaga, M. Murakami, K. Nagai, M. Nakai, H. Nakamura, T. Nakamura, T. Nakazato, Y. Nakao, K. Nishihara, H. Nishimura, T. Norimatsu, P. Norreys, T. Ozaki, J. Pasley, H. Sakagami, Y. Sakawa, N. Sarukura, K. Shigemori, T. Shimizu, A. Sunahara, T. Taguchi, K. Tanaka, K. Tsubakimoto, Y. Fujimoto, H. Homma, and A. Iwamoto, Present status of fast ignition realization experiment and inertial fusion energy development, Nuclear Fusion **53**, 104021 (2013).

[15] Y. Arikawa, S. Kojima, A. Morace, M. Hata, S. Sakata, S. Fujioka, T. Kawashima, Y. Hironaka, K. Shigemori, Y. Abe, Z. Zhang, X. Vaisseau, S. Lee, T. Gawa, K. Matsuo, K. Law, Y. Kato, S. Matsubara, S. Tosaki, A. Yogo, H. Nagatomo, S. Tokita, Y. Nakata, T. Jitsuno, N. Miyanaga, J. Kawanaka, Y. Fujimoto, K. Yamanoi, T. Norimatsu, M. Nakai, H. Nishimura, H. Shiraga, F. GROUP, L. GROUP, H. Azechi, A. Sunahara, T. Johzaki, T. Ozaki, and H. Sakagami, Improvement in the heating efficiency of fast ignition inertial confinement fusion through suppression of the preformed plasma, Nuclear Fusion **57**, 066022 (2017).

[16] L. C. Jarrott, M. S. Wei, C. McGuffey, A. A. Solodov, W. Theobald, B. Qiao, C. Stoeckl, R. Betti, H. Chen, J. Delettrez, T. Döppner, E. M. Giraldez, V. Y. Glebov, H. Habara, T. Iwawaki, M. H. Key, R. W. Luo, F. J. Marshall, H. S. McLean, C. Mileham, P. K. Patel, J. J. Santos, H. Sawada, R. B. Stephens, T. Yabuuchi, and F. N. Beg, Visualizing fast electron energy transport into laser-compressed high-density fast-ignition targets, Nature Physics **12**, 499 (2016).

[17] Y. Kitagawa, Y. Mori, K. Ishii, R. Hanayama, S. Okihara, Y. Arikawa, Y. Abe, E. Miura, T. Ozaki, O. Komeda, H. Suto, Y. Umetani, A. Sunahra, T. Johzaki, H. Sakagami, A. Iwamoto, Y. Sentoku, N. Nakajima, S. Sakata, K. Matsuo, R. S. Mirfayzi, J. Kawanaka, S. Fujiokua, K. Tsubakimoto, K. Shigemori, K. Yamanoi, A. Yogo, A. Nakao, M. Asano, H. Shiraga, T. Motohiro, T. Hioki, and H. Azuma, Direct fast heating efficiency of a counter-imploded core plasma employing a laser for fast ignition experiments (lfex), Nuclear Fusion **62**, 096013 (2022).

[18] R. B. Stephens, H. M. Mclean, W. Theobald, K. Akli, F. N. Beg, Y. Sentoku, D. Schumacher, and M. S. Wei, *Final Project Report "Advanced Concept Exploration For Fast Ignition Science Program"*, Tech. Rep. (University of Rochester, Rochester, NY, 2014).

[19] W. Theobald, A. A. Solodov, C. Stoeckl, K. S. Anderson, R. Betti, T. R. Boehly, R. S. Craxton, J. A. Delettrez, C. Dorrer, J. A. Frenje, V. Y. Glebov, H. Habara, K. A. Tanaka, J. P. Knauer, R. Lauck, F. J. Marshall, K. L. Marshall, D. D. Meyerhofer, P. M. Nilson, P. K. Patel, H. Chen, T. C. Sangster, W. Seka, N. Sinenian, T. Ma, F. N. Beg, E. Giraldez, and R. B. Stephens, Initial cone-in-shell fast-ignition experiments on omega, Physics of Plasmas **18**, 10.1063/1.3566082 (2011).

[20] J. Zhang, W. M. Wang, X. H. Yang, D. Wu, Y. Y. Ma, J. L. Jiao, Z. Zhang, F. Y. Wu, X. H. Yuan, Y. T. Li, and J. Q. Zhu, Double-cone ignition scheme for inertial confinement fusion, Philosophical transactions of the Royal Society A **378**, 20200015 (2020).

[21] Z. Liu, F. Wu, Y. Zhang, X. Yuan, Z. Zhang, X. Xu, Y. Xue, J. Tian, J. Zhong, and J. Zhang, Observation of the colliding process of plasma jets in the double-cone ignition scheme using an x-ray streak camera, Physics of Plasmas **31**, 10.1063/5.0188056 (2024).

[22] P. Norreys, D. Batani, S. Baton, F. N. Beg, R. Kodama, P. Nilson, P. Patel, F. Pérez, J. Santos, R. Scott, V. Tikhonchuk, M. Wei, and J. Zhang, Fast electron energy transport in solid density and compressed plasma, Nuclear Fusion **54**, 054004 (2014).

[23] J. Davies, Electric and magnetic field generation and target heating by laser-generated fast electrons, Physical Review E **68**, 056404 (2003).

[24] A. Robinson and M. Sherlock, Magnetic collimation of fast electrons produced by ultraintense laser irradiation by structuring the target composition, Physics of Plasmas **14**, 083105 (2007).

[25] S. Kar, A. Robinson, D. Carroll, O. Lundh, K. Markey, P. McKenna, P. Norreys, and M. Zepf, Guiding of relativistic electron beams in solid targets by resistively controlled magnetic fields, Physical review letters **102**, 055001 (2009).

[26] B. Ramakrishna, S. Kar, A. P. L. Robinson, D. J. Adams, K. Markey, M. N. Quinn, X. H. Yuan, P. McKenna, K. L. Lancaster, J. S. Green, R. H. H. Scott, P. A. Norreys, J. Schreiber, and M. Zepf, Laser-driven fast electron collimation in targets with resistivity boundary, Physical review letters **105**, 135001 (2010).

[27] F. Pérez, A. Debayle, J. Honrubia, M. Koenig, D. Batani, S. D. Baton, F. N. Beg, C. Benedetti, E. B. S. Chawla, F. Dorchies, C. Fourment, M. Galimberti, L. A. Gizzi, L. Gremillet, R. Heathcote, D. P. Higginson, S. Hulin, R. Jafer, P. Koester, L. Labate, K. L. Lancaster, A. J. MacKinnon, A. G. MacPhee, W. Nazarov, P. Nicolai, J. Pasley, R. Ramis, M. Richetta, J. J. Santos, A. Sgattoni, C. Spindloe, B. Vauzour, T. Vinci, and L. Volpe, Magnetically guided fast electrons in cylindrically compressed matter, Physical review letters **107**, 065004 (2011).

[28] A. Solodov, R. Betti, K. Anderson, J. Myatt, W. Theobald, and C. Stoeckl, Controlling the divergence of laser-generated fast electrons through resistivity gradients in fast-ignition targets, in *Aps meeting abstracts (Nov. 2010)(cit. on p. 166)* (2010).

[29] A. L. Robinson, M. Key, and M. Tabak, Focusing of relativistic electrons in dense plasma using a resistivity-gradient-generated magnetic switchyard, Physical review letters **108**, 125004 (2012).

[30] H. Li, S. Sakata, T. Johzaki, X. Tang, K. Matsuo, S. Lee, K. F. F. Law, Y. Arikawa, Y. Ochiai, C. Liu, J. Nishibata,

https://doi.org/10.1017/hpl.2025.20 Published online by Cambridge University Press

R. Takizawa, H. Morita, H. Azechi, YasuhikoSentoku, and S. Fujioka, Enhanced relativistic electron beams intensity with self-generated resistive magnetic field, High Energy Density Physics **36**, 100773 (2020).

[31] T. Johzaki, K. Yoshitake, T. Endo, W. Kim, S. Fujioka, H. Nagatomo, H. Morita, R. Takizawa, and M. Takemura, Dependence of resistivity gradient guiding of laser-driven relativistic electron beams on laser intensity and duration, Physics of Plasmas **29**, 112707 (2022).

[32] A. Solodov, K. Anderson, R. Betti, V. Gotcheva, J. Myatt, J. Delettrez, S. Skupsky, W. Theobald, and C. Stoeckl, Simulations of electron transport and ignition for direct-drive fast-ignition targets, Physics of Plasmas **15**, 10.1063/1.3000674 (2008).

[33] J. J. Honrubia and J. Meyer-ter Vehn, Fast ignition of fusion targets by laser-driven electrons, Plasma Physics and Controlled Fusion **51**, 014008 (2008).

[34] D. Strozzi, M. Tabak, D. Larson, L. Divol, A. Kemp, C. Bellei, M. Marinak, and M. Key, Fast-ignition transport studies: realistic electron source, integrated particle-in-cell and hydrodynamic modeling, imposed magnetic fields, Physics of Plasmas **19**, 10.1063/1.4739294 (2012).

[35] J. Davies, J. Green, and P. Norreys, Electron beam hollowing in laser-solid interactions, Plasma physics and controlled fusion **48**, 1181 (2006).

[36] S. Y. Gus' kov and P. Kuchugov, Resistivity contribution to stopping power and plasma heating by laser-accelerated electrons, Physics of Plasmas **29**, 122702 (2022).

[37] Y. T. Lee and R. More, An electron conductivity model for dense plasmas, The Physics of fluids **27**, 1273 (1984).

[38] Z. Li, X. Yang, H. Xu, G. Zhang, B. Zeng, S. Chen, Y. Ma, F. Wu, and J. Zhang, Design of laser pulse shapes and target structures by random optimization for direct-drive inertial confinement fusion, Physics of Plasmas **29**, 10.1063/5.0096427 (2022).

[39] H. Song, F. Wu, Z. Sheng, and J. Zhang, Optimization of target compression for high-gain fast ignition via machine learning, Physics of Plasmas **30**, 10.1063/5.0159764 (2023).

[40] T. Tao, G. Zheng, Q. Jia, R. Yan, and J. Zheng, Laser pulse shape designer for direct-drive inertial confinement fusion implosions, High Power Laser Science and Engineering **11**, e41 (2023).

[41] A. Debayle, J. Honrubia, E. d'Humieres, and V. Tikhonchuk, Divergence of laser-driven relativistic electron beams, Physical Review E—Statistical, Nonlinear, and Soft Matter Physics **82**, 036405 (2010).

[42] D. Wu, X. He, W. Yu, and S. Fritzsche, Monte carlo approach to calculate proton stopping in warm dense matter within particle-in-cell simulations, Physical Review E **95**, 023207 (2017).

[43] D. Wu, W. Yu, S. Fritzsche, and X. He, High-order implicit particle-in-cell method for plasma simulations at solid densities, Physical Review E **100**, 013207 (2019).

[44] D. Wu, W. Yu, S. Fritzsche, and X. He, Particle-in-cell simulation method for macroscopic degenerate plasmas, Physical Review E **102**, 033312 (2020).

[45] D. Wu, W. Yu, Y. Zhao, D. Hoffmann, S. Fritzsche, and X. He, Particle-in-cell simulation of transport and energy deposition of intense proton beams in solid-state materials, Physical Review E **100**, 013208 (2019).

[46] K. Nanbu and S. Yonemura, Weighted particles in coulomb collision simulations based on the theory of a cumulative scattering angle, Journal of Computational Physics **145**, 639 (1998).

[47] Y. Sentoku and A. J. Kemp, Numerical methods for particle simulations at extreme densities and temperatures: Weighted particles, relativistic collisions and reduced currents, Journal of computational Physics **227**, 6846 (2008).

[48] F. Pérez, L. Gremillet, A. Decoster, M. Drouin, and E. Lefebvre, Improved modeling of relativistic collisions and collisional ionization in particle-in-cell codes, Physics of Plasmas **19**, 083104 (2012).

[49] A. Gonoskov, Agnostic conservative down-sampling for optimizing statistical representations and pic simulations, Computer Physics Communications **271**, 108200 (2022).

[50] H.-S. Bosch and G. M. Hale, Improved formulas for fusion cross-sections and thermal reactivities, Nuclear fusion **32**, 611 (1992).

[51] T. Ziegler, I. Göthel, S. Assenbaum, C. Bernert, F.-E. Brack, T. E. Cowan, N. P. Dover, L. Gaus, T. Kluge, S. Kraft, F. Kroll, J. Metzkes-Ng, M. Nishiuchi, I. Prencipe, T. Püschel, M. Rehwald, M. Reimold, H.-P. Schlenvoigt, M. E. P. Umlandt, M. Vescovi, U. Schramm, and K. Zeil, Laser-driven high-energy proton beams from cascaded acceleration regimes, Nature Physics , 1 (2024).

[52] M. Nishiuchi, N. P. Dover, M. Hata, H. Sakaki, K. Kondo, H. F. Lowe, T. Miyahara, H. Kiriyama, J. K. K. N. Iwata, M. A. Alkhimova, A. S. Pirozhkov, A. Y. Faenov, T. A. Pikuz, A. Sagisaka, Y. Watanabe, M. Kando, K. Kondo, E. J. Ditter, O. C. Ettlinger, G. S. Hicks, Z. Najmudin, T. Ziegler, K. Zeil, U. Schramm, and Y. Sentoku, Dynamics of laser-driven heavy-ion acceleration clarified by ion charge states, Physical Review Research **2**, 033081 (2020).

[53] D. Gorlova, A. Y. Zavorotny, I. Tsymbalov, K. Ivanov, S. Shulyapov, R. Volkov, and A. Savel'ev, Neutron source from (γ, n) reactions at a laser-plasma accelerator and its use for electron beam characterization, Journal of Surface Investigation: X-ray, Synchrotron and Neutron Techniques **17**, 865 (2023).

[54] Y. T. Li, C. Li, M. L. Zhou, W. M. Wang, F. Du, W. J. Ding, X. X. Lin, F. Liu, Z. M. Sheng, X. Y. Peng, L. M. Chen, J. L. Ma, X. Lu, Z. H. Wang, Z. Y. Wei, and J. Zhang, Strong terahertz radiation from relativistic laser interaction with solid density plasmas, Applied Physics Letters **100**, 10.1063/1.4729874 (2012).

[55] S. Herzer, A. Woldegeorgis, J. Polz, A. Reinhard, M. Almassarani, B. Beleites, F. Ronneberger, R. Grosse, G. G. Paulus, U. Hübner, T. May, and A. Gopal, An investigation on thz yield from laser-produced solid density plasmas at relativistic laser intensities, New Journal of Physics **20**, 063019 (2018).

[56] W.-M. Wang, P. Gibbon, Z.-M. Sheng, and Y.-T. Li, Magnetically assisted fast ignition, Physical review letters **114**, 015001 (2015).

[57] A. Solodov and R. Betti, Stopping power and range of energetic electrons in dense plasmas of fast-ignition fusion targets, Physics of Plasmas **15**, 042707 (2008).

[58] G. Faussurier and C. Blancard, Resistivity saturation in warm dense matter, Physical Review E **91**, 013105 (2015).

[59] N. Wetta and J.-C. Pain, Consistent approach for electrical resistivity within ziman's theory from solid state to hot dense plasma: Application to aluminum, Physical

https://doi.org/10.1017/hpl.2025.20 Published online by Cambridge University Press

Review E **102**, 053209 (2020).

[60] R. Mishra, P. Leblanc, Y. Sentoku, M. Wei, and F. Beg, Collisional particle-in-cell modeling for energy transport accompanied by atomic processes in dense plasmas, Physics of Plasmas **20**, 072704 (2013).

[61] B. He and J.-G. Wang, Stopping power for alpha particles in hot dense au plasmas, Nuclear Fusion **53**, 093009 (2013).

https://doi.org/10.1017/hpl.2025.20 Published online by Cambridge University Press